Journal of Materials Chemistry A

Accepted Manuscript

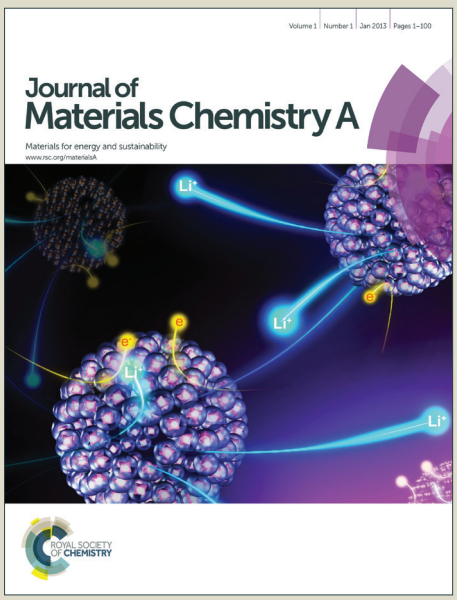

ROYAL SOCIETY OF CHEMISTRY

www.rsc.org/materialsA

Journal Name

RSCPublishing

ARTICLE

Mechano-chemical Synthesis of Nanostructured $FePO_4$/MWCNTs Composites as Cathode Materials for Lithium-ion Batteries

Cite this: DOI: 10.1039/x0xx00000x

Received 00th January 2014,
Accepted 00th January 2014

DOI: 10.1039/x0xx00000x

www.rsc.org/

Hui Dou,[a,b] Ping Nie,[a] and Douglas R. MacFarlane[*b]

Nanostructured iron phosphate/multi-walled carbon nanotubes ($FePO_4$/MWCNTs) composites have been synthesized by a mechano-chemical process using 1-butyl-3-methylimidazolium tetrachloroferrate (bmim$FeCl_4$) and $(NH_4)_3PO_4 \cdot 3H_2O$ as precursors in the presence of 1-butyl-3-methylimidazolium chloride (bmimCl). The bmim$FeCl_4$ serves not only to provide the necessary Fe-ion source, but also as a co-dispersant for the MWCNTs and as a soft co-template for structure control of the $FePO_4$ nanoparticles, together with the bmimCl. The obtained $FePO_4$/MWCNTs composites were characterized by Fourier transform infrared spectroscopy (FTIR), X-ray diffraction (XRD), scanning electron microscopy (SEM), transmission electron microscopy (TEM), thermogravimetric and differential scanning calorimetry analysis (TG-DSC). As cathode materials for rechargeable lithium-ion batteries, the composites exhibited capacity of 171 mAh g^{-1} at a current density of 40 mA g^{-1}, which is close to theoretical capacity for this material, and good cycle performance, with a reversible capacity of 135 mAh g^{-1} after 100 cycles at a rate of 50 mA g^{-1}.

Introduction

Rechargeable lithium-ion batteries (LIBs) are the leading power sources for portable electronic devices, electric vehicles and hybrid electric vehicles owing to their high energy density, light weight, and long service life.[1-3] Electrode materials operating in these devices are important components in determining their performance. Amorphous $FePO_4 \cdot nH_2O$ ($0 \le n \le 4$) has been actively investigated as a potential cathode material because it can provide charge-discharge capacity as high as 178 mAh g^{-1} in its dehydrated state.[4, 5] However, the practical specific capacity of $FePO_4$ is quite low due to the sluggish kinetics of the lithium intercalation-extraction process and the low electronic conductivity.[6] Consequently, nanoengineering,[7-10] morphology control [11-13] and mixing the particles with various carbon additives[14-18] have all been investigated in the literature to improve the reversible capacity and rate capability of $FePO_4$ electrodes. Amorphous $FePO_4$ hollow nanospheres with tunable shell thickness were synthesized by a simple hydrothermal approach.[12] The electrodes exhibited good electrochemical performance with high specific capacity, rate capability, and excellent cyclablilty in lithium ion batteries. Porous $FePO_4$ nanotubes have been prepared by an oil-phase synthesis using Fe_2O_3 nanotubes as new precursors and templates. Galvanostatic discharge-charge cycling showed that the porous nanotubes could maintain a reversible specific capacity of 130.3 mAh g^{-1} after 35 cycles at a current density of 0.2C.[13] Cai *et al.*[17] reported a graphene-amorphous $FePO_4$ composite as a cathode for lithium ion batteries. The electrode showed initial discharge capacity of 174 mAh g^{-1} and maintained approximately 98% capacity at a current density of 20 mA g^{-1}. Moreover, $FePO_4$ has recently been investigated as promising candidates in sodium-ion batteries. A maize-like $FePO_4$@MCNT nanowire composite delivered a capacity of 157.2 mAh g^{-1} after 70 cycles at a current of 0.1C, and also exhibited high rate capability.[19] Hu *et al.* [20] reported a simple hydrothermal method to produce a networked nanocomposite of single-wall carbon nanotubes/amorphous porous $FePO_4$ nanoparticles, which showed a discharge capacity of 120 mAh g^{-1} at 10 mA g^{-1} as cathode for sodium ion batteries. Very recently, mesoporous amorphous $FePO_4$ nanospheres have been synthesized through a simple chemically induced precipitation method [21]. When tested as cathodes for sodium storage, the materials demonstrate a high initial discharge capacity of 151 mAh g^{-1} at 20 mA g^{-1} and excellent cyclablilty with 94% capacity retention after 160 cycles.

Various synthetic methods have been reported for the preparation of $FePO_4$.[4, 20, 22, 23] However, many of these procedures suffer from complex processing and low production rates. As mostly reported in the literature, $FePO_4$ is usually prepared by a precipitation route *via* addition of a solution of phosphate to that of an iron (III) salt. The as-prepared product is the hydrated $FePO_4$, which delivers lower capacity and needs to be further calcined at high temperature to form a dehydrated product.[24, 25] Furthermore, since Fe^{3+} is prone to hydrolysis, the reaction has to be carried out at very low pH (1.5), which makes the synthesis time consuming, even up to a week. Also the use of strong acid and base causes not only the corrosion of the facilities in industry, but also potential environmental issues. Therefore, it is highly desirable to prepare $FePO_4$ with improved electrochemical performance using a simple and environmentally benign synthesis process.

Imidazolium-based ionic liquids were discovered to be capable of effectively disentangling carbon nanotubes (CNTs) clusters *via* interaction between the imidazolium cations and the π-electrons of the CNTs surface, resulting in the formation of gelatinous materials.[26, 27] Inspired by these advantages, a new facile and environmentally benign synthesis of nanostructured $FePO_4$/multi-walled carbon nanotubes ($FePO_4$/MWCNTs) composites has been developed in the present work by mechanical ball milling using 1-butyl-3-methylimidazolium tetrachloroferrate (bmim$FeCl_4$) ionic liquid and $(NH_4)_3PO_4{\cdot}3H_2O$ as precursors in the presence of 1-butyl-3-methylimidazolium chloride (bmimCl) ionic liquid. The bmim$FeCl_4$ serves not only as reagent to provide the necessary Fe-ion source, but also as a co-dispersant for the MWCNTs and a co-soft template for nanostructure control of the $FePO_4$, together with bmimCl. The lithium storage performance of the $FePO_4$/MWCNTs materials as cathodes was also studied. The short solid-state pathway for Li^+ diffusion, as well as the three-dimensional MWCNTs network for electron transfer, enables rapid lithium ion de/intercalation. The resultant material exhibits a reversible discharge capacity of 171 mAh g^{-1} at a current density of 40 mA g^{-1} as well as excellent cycling stability with 93.3% capacity retention over 100 cycles.

Results and discussion

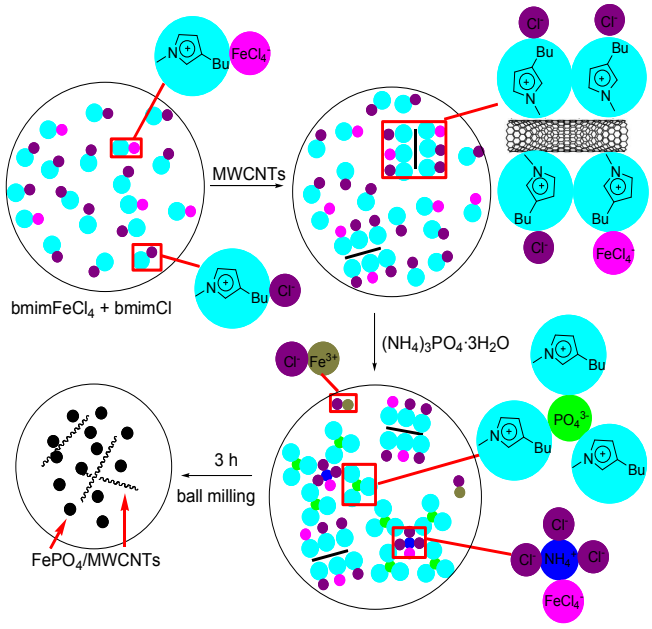

Scheme 1 Schematic illustration of the synthesis mechanism of the $FePO_4$/MWCNTs.

Scheme 1 shows a possible synthesis mechanism of the nanostructured $FePO_4$/MWCNTs composites. The MWCNTs are dispersed into the ionic liquid mixture of bmim$FeCl_4$ and bmimCl *via* "cation-π" interaction between the imidazolium cations and the π-electrons of the MWCNTs surface, resulting in the formation of a Bucky-gel.[26, 27] The $(NH_4)_3PO_4{\cdot}3H_2O$ is incorporated into the gel *via* ion interaction by mechanical ball milling.[28, 29] Equilibrium between $FeCl_4^-$ and Fe^{3+}, allows the precipitation of $FePO_4$ from the mixture, where the nano-grains are well separated due to the interfacial tension.[30, 31]

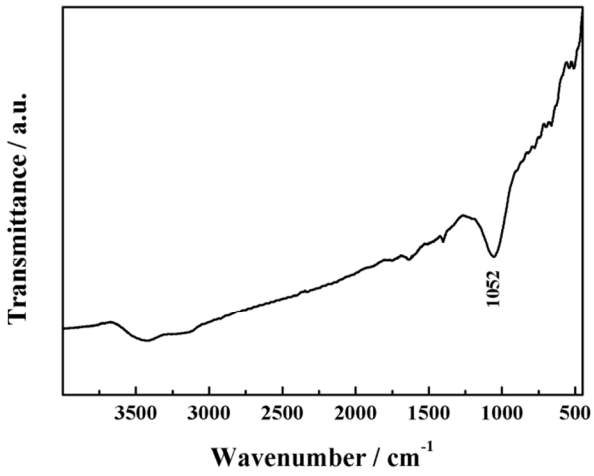

Fig. 1 FTIR spectroscopy of $FePO_4$/MWCNTs.

The composition of the as-obtained material was identified by Fourier transform infrared spectroscopy (FTIR) and X-ray diffraction (XRD). In the FTIR spectroscopy of the $FePO_4$/MWCNTs composites shown in Fig. 1, a strong absorption peak at around 1052 cm^{-1} can be assigned to Fe-O-P bonding, indicating the formation of $FePO_4$, which is in agreement with previous reports.[11, 32] No intense peak can be detected in the XRD pattern of the $FePO_4$/MWCNTs composites shown in Fig. 2, which suggests the amorphous nature of the sample. This is critical to its electrochemical properties since amorphous $FePO_4$ is electrochemically active while the crystalline $FePO_4$ is less active.[25] Diffraction peaks from the MWNTs also cannot be detected, which may be attributed to the small content of MWNTs in the composites.

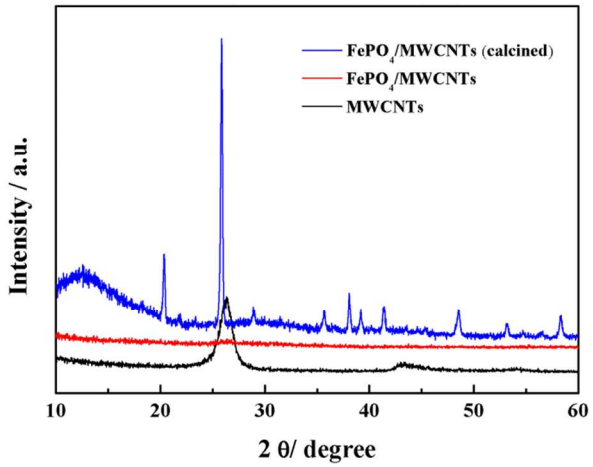

Fig. 2 XRD patterns of MWCNTs, $FePO_4$/MWCNTs and calcined $FePO_4$/MWCNTs.

After calcination at 800℃ for 5 h, the XRD pattern of the $FePO_4$/MWCNTs composite shows the characteristic diffraction peaks located at 20.37°, 25.86°, 35.68°, 38.04°, 39.20°, 41.37°, 48.56°, 53.13° and 58.33°, indicating the hexagonal $FePO_4$ (JCPDS card No. 29-0715). A tiny diffraction peak at 29.02 can be ascribed to Fe_3PO_7 (JCPDF card No. 00-050-1634) which might come from the hydrolysis of bmim$FeCl_4$ residue absorbed on the surface of the $FePO_4$/MWCNTs composites. A small amount of bmim$FeCl_4$

residue could hydrolyze to produce $Fe(OH)_3$ when washed with distilled water; in the process of calcination, $Fe(OH)_3$ dehydrates to form FeOOH and then Fe_2O_3 which could continue to react with $FePO_4$ to yield Fe_3PO_7.[33] The average crystallite size of the calcined $FePO_4$/MWCNTs deduced from Scherrer's equation for the strongest peak (102) can be estimated to be 49 nm.

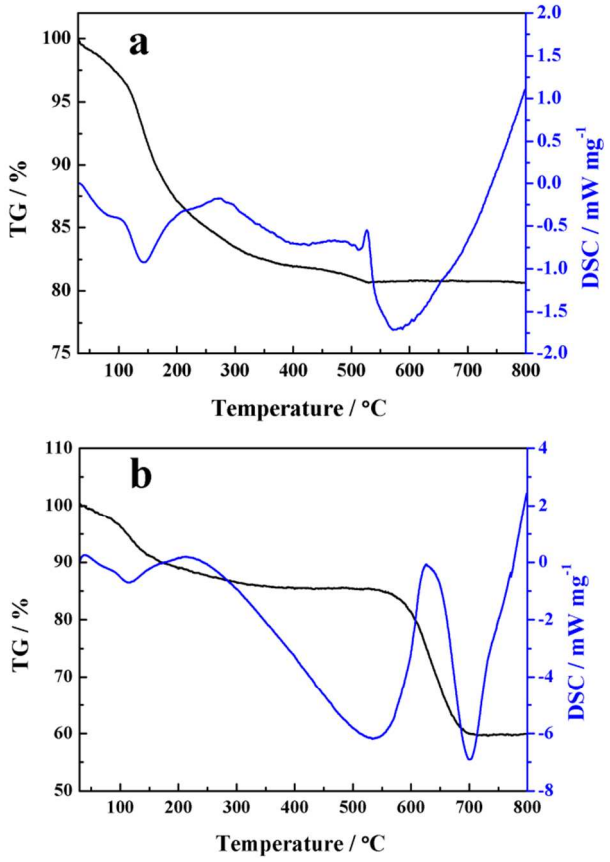

Fig. 3 TG and DSC curves of $FePO_4$ (a) and $FePO_4$/MWCNTs composites (b).

The thermogravimetric (TG) analyses were carried out to investigate the behavior of the $FePO_4$ and $FePO_4$/MWCNTs materials during heating treatment, as presented in Fig. 3. In Fig. 3a, the weight loss of about 3% from 30-105 ℃ can be ascribed to the loss of retained water in the $FePO_4$. The endothermic peak around 150℃ with a weight loss of about 11% from 105-250℃ corresponds to the elimination of one water molecule per formula unit. This indicates a chemical composition of $FePO_4 \cdot H_2O$, which could deliver a higher theoretical capacity than $FePO_4$ obtained by co-precipitation in solution which typically has at least two hydrate waters per mole of compound. Because the obvious decomposition of bmimCl appears at about 250℃[34, 35], a slight weight loss of about 2% from 250 to 300 ℃ might be attributed to the elimination of residual components of bmimCl absorbed on the surface of the $FePO_4$/MWCNTs composites.[26, 27, 30] At 530 ℃, a small exothermic peak appears which can be attributed to the structural transformation from amorphous to hexagonal $FePO_4$.[36, 37] In Fig. 3b, the weight loss of about 13% below 300 ℃ corresponds to the removal of absorbed and structural water, and decomposition of residual bmimCl in the $FePO_4$/MWCNTs. The MWCNTs content in the composites is estimated to be approximately 25.6% according to the sharp weight loss between 500 ℃ and 700 ℃, which is similar to that of $FePO_4$/CNTs composites reported in the literature.[15, 24]

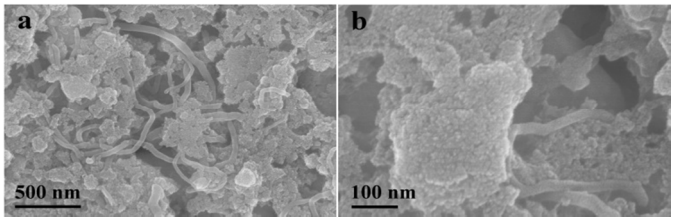

Fig. 4 SEM images of $FePO_4$/MWCNTs.

The detailed structure and morphology were analyzed by field emission scanning electron microscopy (SEM) and transmission electron microscopy (TEM). The SEM images of the $FePO_4$/MWCNTs shown in Fig. 4 indicate that small $FePO_4$ nanoparticles appear to be interconnected with each other to form porous agglomerates. The MWCNTs uniformly disperse into the agglomerates of $FePO_4$ forming a highly conductive network. TEM images of the $FePO_4$/MWCNTs are illustrated in Fig. 5. The light regions in Fig 5a and 5b clearly reveal the presence of the interparticle voids in the loose agglomerates, which is beneficial to electrochemical utilization and facilitates electrolyte penetration. The HR-TEM image shown in Fig. 5c shows no discernible lattice fringes. The selected area electron diffraction (SAED) pattern in Fig. 5d further confirms the amorphous state of the nanoparticles.

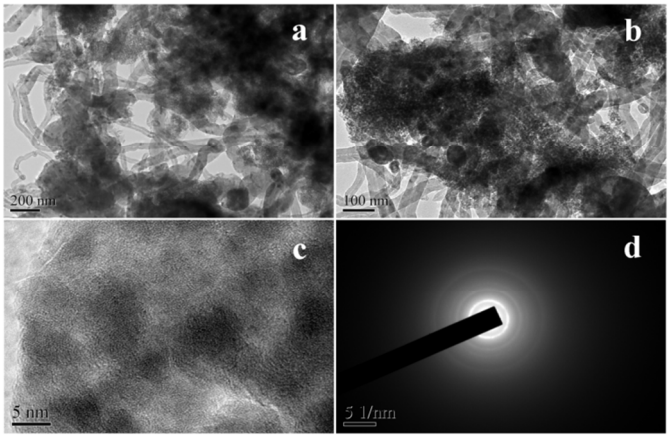

Fig. 5 TEM and HRTEM images of $FePO_4$/MWCNTs.

The electrochemical performance of the as-prepared $FePO_4$/MWCNTs composites were evaluated by cyclic voltammetry (CV) and galvanostatic charge/discharge tests shown in Fig. 6. The CV curve in Fig. 6a shows a pair of reduction/oxidation peaks at about 2.63 and 2.98 V within a wide voltage range from 2.0 to 4.2 V in a 1 M $LiPF_6$ EC/DMC electrolyte solution at a scan rate of 0.1 mV s^{-1}, corresponding to the Li insertion/extraction processes in the $FePO_4$/MWCNTs. The initial ten discharge-charge profiles of the $FePO_4$/MWCNTs electrode at a current density of 40 mA g^{-1} are presented in Fig. 6b. The potential increases (or decreases) smoothly with the evolution of lithium ion insertion and extraction, showing the well-known signature of voltage trends for the $FePO_4$ electrode. The initial discharge capacity is 143 mAh g^{-1}, and the reversible capacity increases to approximately 171 mAh g^{-1} after 9 cycles. This is very close to its theoretical

value of 178 mAh g^{-1}, indicating full utilization of the active material.

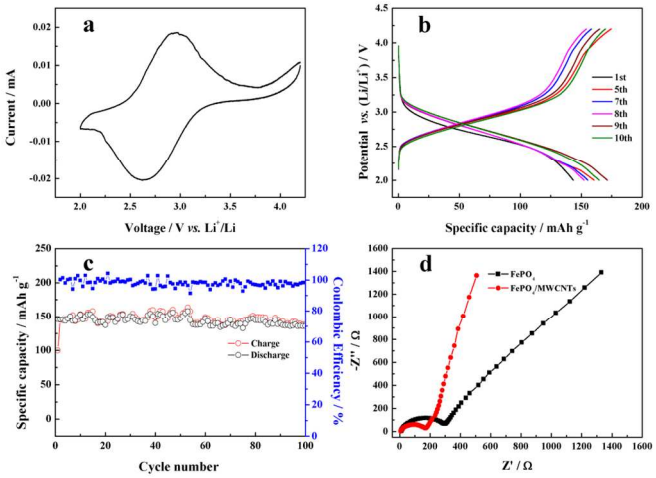

Fig. 6 Electrochemical performance of the $FePO_4$/MWCNTs as cathode materials for Li ion batteries in the voltage range of 2.0-4.2 V: (a) the CV curve at a scan rate of 0.1 mV s^{-1}, (b) charge/discharge curves at a current density of 40 mA g^{-1}, (c) cycling performance and Coulombic efficiency at a current density of 50 mA g^{-1}, (d) EIS spectra of the $FePO_4$ and $FePO_4$/MWCNTs.

Due to the presence of ionic liquid residue on the surface of the $FePO_4$/MWCNTs, the slightly increasing capacity for the $FePO_4$/MWCNTs found during several initial cycles may be caused by the electrode-electrolyte interface activation[38] and Li channel development due to the repeated lithiation/delithiation reaction.[32, 39] Fig. 6c shows the cycling performance and Coulombic efficiency at a current density of 50 mA g^{-1}. At this higher rate the $FePO_4$/MWCNTs deliver charge/discharge capacities as high as 145/145 mAh g^{-1} in the second cycle. A reversible capacity of 135 mAh g^{-1} is still achieved after 100 cycles, corresponding to 93.3% of the second cycle discharge capacity. In addition, the Coulomb efficiency remains at almost 100% during all the cycles, thus indicating excellent cycling stability and reversibility. It should be noted that the lithium storage properties of the $FePO_4$/MWCNTs in terms of specific capacity and cycling performance are comparable or even superior to the reported $FePO_4$ cathode materials in the literature.[6, 40-43]

The outstanding lithium storage properties of these $FePO_4$/MWCNTs can be attributed to the unique structure of the material. The ultrafine $FePO_4$ nanoparticles create shorter distances for transportation of Li ions within the material ensuring full and uniform utilization of the material. The porous agglomerate of $FePO_4$ nano-particles also facilitates electrolyte infiltration, optimizing the ion diffusion characteristics of the electrode. The carbon nanotube network facilitates fast electron transfer, leading to a lower material resistance. Fig. 6d shows the EIS spectra of the $FePO_4$ and $FePO_4$/MWCNTs. The diameter of the semicircle for the $FePO_4$/MWCNTs composites in the high-medium frequency region is much smaller than that of pure $FePO_4$, revealing lower contact and charge transfer resistances.[15] This indicates that the electronic conductivity of the $FePO_4$/MWCNTs is significantly improved by the MWCNTs nets, giving the $FePO_4$/MWCNTs high specific capacities and good cycling performance. In addition, we also compared this work with other $FePO_4$/CNTs composites reported in the recent literature, and the results are shown in Table S1.

Conclusions

In this work, nanostructured $FePO_4$/MWCNTs composites were successfully prepared through a mechano-chemical ball-milling process using $bmimFeCl_4$ as a Fe-ion source in the presence of bmimCl. Both $bmimFeCl_4$ and bmimCl can serve as dispersants for MWCNTs and soft templates for structural control of the $FePO_4$ nanoparticles. The as-prepared $FePO_4$/MWCNT performed very well as a cathode material for rechargeable Li ion batteries in terms of specific capacity and capacity retention. Furthermore, compared with conventional methods used in the synthesis of transition metal phosphate nanostructures, our approach utilizing a Fe-containing ionic liquid is somewhat more environmentally friendly as it requires no additional reagents.

Experimental

Material Synthesis

The ionic liquid bmimCl (≥95%) was produced by Badische Anilin-und-Soda-Fabrik (Germany). The ionic liquid $bmimFeCl_4$ was synthesized according to a reported procedure.[44] MWCNTs with the diameter of 20-40 nm and length of less than 2 μm were purchased from Shenzhen Nanotech Port Co., Ltd (China) and purified according to the previous report [45] with some modification: 2 g of the MWCNTs was refluxed in 60 mL of HNO_3 (65 wt.%) at 80 ℃ for 24 h. Afterward, the acid treated MWCNTs were rinsed with distilled water until a neutral pH value, collected by filtration, and then dried in vacuum at 60 ℃ for further use. No further calcination or annealing was required, except for samples for XRD analysis, which we calcined at 800°C. Other chemicals are of analytical grade and employed directly without further purification.

The $FePO_4$/MWCNTs composites were synthesized by mechanical ball milling using $bmimFeCl_4$ and $(NH_4)_3PO_4{\cdot}3H_2O$ as precursors in the presence of bmimCl. Initially, MWCNTs (57 mg) were milled with $bmimFeCl_4$ (1 mmol) and bmimCl (1 ml) at 120 rpm for 2 h using a high-energy mechanical mill (FRITSCH, PULVERISETTE 6). After that, $(NH_4)_3PO_4{\cdot}3H_2O$ (1 mmol) was added into the mixture and milled at 300 rpm for 3 h. The product was collected by centrifugation and washed with absolute ethanol and then de-ionized water several times. The as-obtained $FePO_4$/MWCNTs composites were dried in vacuum at 60 °C for 12 h. In addition, pristine $FePO_4$ nanoparticles were also prepared through the same procedure without adding any MWCNTs.

Material Characterization

The chemical composition of the as-prepared products was characterized by powder X-ray diffraction (Bruker D8 advance) using Cu K_α radiation. The calcination of the samples was performed in air atmosphere for 5 h after heating to 800 ℃ from room temperature at a heating rate of 10 ℃ min^{-1}. The morphology of the samples was investigated by field-emission scanning electron microscopy (FESEM, LEO 1430VP, Germany) and transmission electron microscopy (TEM, JEOL JEM-2100). Thermogravimetric and differential scanning calorimetry analysis (TG-DSC) was conducted simultaneously on a TG-DSC instrument (NETZSCH STA 409 PC) under air flow from room temperature to 800 ℃ at a heating rate of 10 ℃

min^{-1}. Fourier transform infrared spectroscopy (FTIR) spectrum was recorded on a Nicolet 750 Fourier transform infrared spectrometer using the KBr pellet method.

Electrochemical Tests

The electrochemical measurements utilized a 2016-type coin cell with pure lithium metal as the reference electrode. The working electrodes were prepared by mixing active material, acetylene black and polyvinylidenedifluoride (PVDF) in a weight ratio of 80:10:10 in *N*-methyl pyrrolidinone (NMP). The slurry was then spread onto an aluminum foil and dried under vacuum at 110 ℃ for 12 h. The cell assembly was performed in an argon-filled glove box. The electrolyte used was 1 M $LiFP_6$ dissolved in a mixture of ethylene carbonate (EC) and dimethyl carbonate (DMC) (1:1 v/v). Cyclic voltammetry (CV) was studied using an electrochemical workstation (CHI 750D) in the potential range 2.0-4.2 V at a scan rate of 0.1 mV s^{-1}. Galvanostatic charge/discharge tests were performed using a Land Battery Test System (Wuhan, China) over a potential range of 2.0-4.2 V *vs.* Li^+/Li. Electrochemical impendence spectroscopy (EIS) was obtained by using a CHI 750D electrochemical workstation with amplitude of 5 mV in the frequency range from 100 kHz to 0.01 Hz.

Acknowledgements

This work was supported by the National Natural Science Foundation of China (No. 21103091, 21173120, 51372116), National Basic Research Program of China (973 Program) (No. 2014CB239701), Natural Science Foundation of Jiangsu Province (BK2011030), and Fundamental Research Funds for the Central Universities (NP2014403). DRM is grateful to the Australian Research Council for support as an Australian Laureate Fellow.

Notes and references

[a]College of Material Science and Engineering, Nanjing University of Aeronautics and Astronautics, Nanjing, China

[b]Australian Centre for Electromaterials Science, Monash University, Clayton, Victoria 3800, Australia. Fax: +61-3-99054597; Tel: +61-3-99054540; E-mail: douglas.macfarlane@monash.edu

Electronic Supplementary Information (ESI) available: [supplementary table: Table S1]. See DOI: 10.1039/b000000x/

1. J. M. Tarascon and M. Armand, *Nature*, 2001, **414**, 359-367.
2. M. Armand and J. M. Tarascon, *Nature*, 2008, **451**, 652-657.
3. J. S. Chen, L. A. Archer and X. Wen Lou, *J. Mater. Chem.*, 2011, **21**, 9912-9924.
4. P. P. Prosini, M. Lisi, S. Scaccia, M. Carewska, F. Cardellini and M. Pasquali, *J. Electrochem. Soc.*, 2002, **149**, A297-A301.
5. Y. Song, S. Yang, P. Y. Zavalij and M. S. Whittingham, *Mater. Res. Bull.*, 2002, **37**, 1249-1257.
6. Z. C. Shi, A. Attia, W. L. Ye, Q. Wang, Y. X. Li and Y. Yang, *Electrochim. Acta*, 2008, **53**, 2665-2673.
7. Y.-S. Hong, K. S. Ryu, Y. J. Park, M. G. Kim, J. M. Lee and S. H. Chang, *J. Mater. Chem.*, 2002, **12**, 1870-1874.
8. C. Delacourt, P. Poizot, S. Levasseur and C. Masquelier, *Electrochem. Solid-State Lett.*, 2006, **9**, A352-A355.
9. D.-H. Kim and J. Kim, *Electrochem. Solid-State Lett.*, 2006, **9**, A439-A442.
10. Y. Lu, T. Zhang, Y. Liu and G. Luo, *Chem. Eng. J.*, 2012, **210**, 18-25.
11. J. Zhao, Z. Jian, J. Ma, F. Wang, Y.-S. Hu, W. Chen, L. Chen, H. Liu and S. Dai, *ChemSusChem*, 2012, **5**, 1495-1500.
12. Y. Yin, P. Wu, H. Zhang and C. Cai, *Electrochem. Commun.*, 2012, **18**, 1-3.
13. R. Cai, Y. Du, W. Zhang, H. Tan, T. Zeng, X. Huang, H. Yang, C. Chen, H. Liu, J. Zhu, S. Peng, J. Chen, Y. Zhao, H. Wu, Y. Huang, R. Xu, T. M. Lim, Q. Zhang, H. Zhang and Q. Yan, *Chem. - Eur. J.*, 2013, **19**, 1568-1572.
14. Y. J. Lee, H. Yi, W.-J. Kim, K. Kang, D. S. Yun, M. S. Strano, G. Ceder and A. M. Belcher, *Science*, 2009, **324**, 1051-1055.
15. C. X. Guo, Y. Q. Shen, Z. L. Dong, X. D. Chen, X. W. Lou and C. M. Li, *Energy Environ. Sci.*, 2012, **5**, 6919-6922.
16. S.-W. Kim, J. Ryu, C. B. Park and K. Kang, *Chem. Commun.*, 2010, **46**, 7409-7411.
17. Y. Yin, Y. Hu, P. Wu, H. Zhang and C. Cai, *Chem. Commun.*, 2012, **48**, 2137-2139.
18. L. Chen, P. Wu, K. Xie, J. Li, B. Xu, G. Cao, Y. Chen, Y. Tang, Y. Zhou, T. Lu and Y. Yang, *Electrochim. Acta*, 2013, **92**, 433-437.
19. S. Xu, S. Zhang, J. Zhang, T. Tan and Y. Liu, *J. Mater. Chem. A*, 2014, **2**, 7221-7228.
20. Y. Liu, Y. Xu, X. Han, C. Pellegrinelli, Y. Zhu, H. Zhu, J. Wan, A. C. Chung, O. Vaaland, C. Wang and L. Hu, *Nano Lett.*, 2012, **12**, 5664-5668.
21. Y. Fang, L. Xiao, J. Qian, X. Ai, H. Yang and Y. Cao, *Nano Lett.*, 2014, **14**, 3539-3543.
22. Z. Shi, Y. Li, W. Ye and Y. Yang, *Electrochem. Solid-State Lett.*, 2005, **8**, A396-A399.
23. N. Rajić, R. Gabrovšek and V. Kaučič, *Thermochim. Acta*, 2000, **359**, 119-122.
24. J.-P. Jegal, J.-G. Kim and K.-B. Kim, *Electrochem. Commun.*, 2013, **30**, 87-90.
25. J. Ryu, S.-W. Kim, K. Kang and C. B. Park, *Adv. Mater.*, 2010, **22**, 5537-5541.
26. T. Fukushima and T. Aida, *Chem. - Eur. J.*, 2007, **13**, 5048-5058.
27. T. Fukushima, A. Kosaka, Y. Ishimura, T. Yamamoto, T. Takigawa, N. Ishii and T. Aida, *Science*, 2003, **300**, 2072-2074.
28. C. Zhang, J. Chen, Y. Zhou and D. Li, *J. Phys. Chem. C*, 2008, **112**, 10083-10088.
29. A. Chaumont and G. Wipff, *Phys. Chem. Chem. Phys.*, 2003, **5**, 3481-3488.
30. C. Li, L. Gu, J. Tong and J. Maier, *ACS Nano*, 2011, **5**, 2930-2938.
31. C. Li, C. Yin, L. Gu, R. E. Dinnebier, X. Mu, P. A. van Aken and J. Maier, *J. Am. Chem. Soc.*, 2013, **135**, 11425-11428.
32. H. Kim, S.-W. Kim, J. Hong, H.-D. Lim, H. S. Kim, J.-K. Yoo and K. Kang, *J. Electrochem. Soc.*, 2011, **158**, A930-A935.
33. Y.-S. Hong, Y. J. Park, K. S. Ryu and S. H. Chang, *Solid State Ionics*, 2003, **156**, 27-33.
34. C. P. Fredlake, J. M. Crosthwaite, D. G. Hert, S. N. V. K. Aki and J. F. Brennecke, *J. Chem. Eng. Data*, 2004, **49**, 954-964.
35. K. Prasad, Y. Kaneko and J.-i. Kadokawa, *Macromol. Biosci.*, 2009, **9**, 376-382.
36. W.-j. Cui, H.-j. Liu, C.-x. Wang and Y.-y. Xia, *Electrochem. Commun.*, 2008, **10**, 1587-1589.
37. S. Okada, T. Yamamoto, Y. Okazaki, J.-i. Yamaki, M. Tokunaga and T. Nishida, *J. Power Sources*, 2005, **146**, 570-574.
38. T. R. Kim, D. H. Kim, H. W. Ryu, J. H. Moon, J. H. Lee, S. Boo and J. Kim, *J. Phys. Chem. Solids*, 2007, **68**, 1203-1206.

39. C. Li, L. Gu, S. Tsukimoto, P. A. van Aken and J. Maier, *Adv. Mater.*, 2010, **22**, 3650-3654.
40. C. Gerbaldi, G. Meligrana, S. Bodoardo, A. Tuel and N. Penazzi, *J. Power Sources*, 2007, **174**, 501-507.
41. G.-n. Hao, H. Zhang, X.-H. Chen, G.-P. Cao and Y. Yang, *Mater. Res. Bull.*, 2012, **47**, 4048-4053.
42. Y. J. Lee and A. M. Belcher, *J. Mater. Chem.*, 2011, **21**, 1033-1039.
43. R. Cai, H. Liu, W. Zhang, H. Tan, D. Yang, Y. Huang, H. H. Hng, T. M. Lim and Q. Yan, *Small*, 2013, **9**, 1036-1041.
44. M. S. Sitze, E. R. Schreiter, E. V. Patterson and R. G. Freeman, *Inorg. Chem.*, 2001, **40**, 2298-2304.
45. Z. Wang, D. Luan, S. Madhavi, Y. Hu and X. W. Lou, *Energy Environ. Sci.*, 2012, **5**, 5252-5256.

Table of contents entry

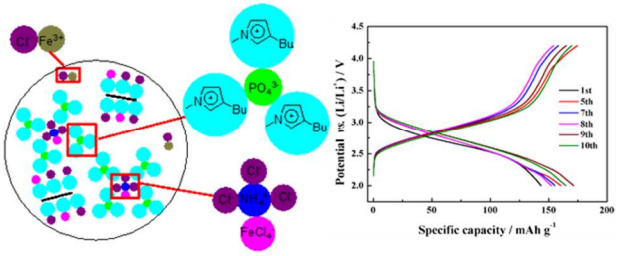

Nanostructured $FePO_4$/MWCNTs composites as promising cathode candidates for lithium-ion batteries have been environmentally synthesized by a mechano-chemical process using 1-butyl-3-methylimidazolium tetrachloroferrate (bmim$FeCl_4$) as a precursor in the presence of 1-butyl-3-methylimidazolium chloride (bmimCl).